JOURNAL OF AIRCRAFT
Vol. 33, No. 5, September–October 1996

Aircraft Anti-Icing and De-Icing Techniques and Modeling

Scott K. Thomas and Robert P. Cassoni
Wright State University, Dayton, Ohio 45435
and
Charles D. MacArthur
U.S. Air Force Wright Laboratory, Wright–Patterson Air Force Base, Ohio 45433

Nomenclature

A_c = accumulation parameter
C_d = drag coefficient
C_l = lift coefficient
C_m = moment coefficient
C_p = pressure coefficient
c = specific heat at constant pressure, J/(kg-K); airfoil chord, m
D = propeller diameter, m; flexural stiffness, N-m
$\boldsymbol{D}$ = drag force, N
d = droplet diameter, m
E = total collection efficiency
f = freezing fraction
g = acceleration caused from gravity, m/s^2
H_i = ice thickness, m
H_p = plate thickness, m
h = airfoil projected height, m
h_c = convective heat transfer coefficient, W/(m^2-K)
h_{fg} = heat of vaporization, J/kg
h_{sl} = heat of fusion, J/kg
I = airfoil drag constant
K = thermal conductivity, W/(m-K); inertia parameter
K_0 = modified inertia parameter
k = roughness diameter, m
LWC = liquid water content, kg/m^3
M = local Mach number
MVD = median volume droplet diameter, m
m = mass, kg
$\dot{m}$ = mass flow rate, kg/s
$\dot{m}'$ = mass flow rate per unit width, kg/(m-s)
$\dot{m}''$ = mass flux, kg/(m^2-s)
n = normal direction
P = pressure, Pa
p = spatial pressure distribution, N/m^2
$\dot{Q}$ = heat rate, W
q = normal pressure distribution, N/m^2

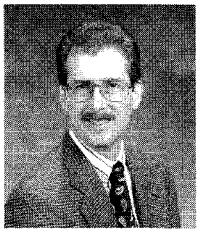

Scott K. Thomas is an Assistant Professor of Mechanical Engineering at Wright State University. He received his Ph.D. from the University of Dayton in 1993, and has published 18 journal articles and conference papers. His recent research interests include the effects of transient acceleration fields on axially grooved heat pipes, loop heat pipes, and thermosyphons. This research is aimed at the application of passive two-phase heat transfer devices to civil and military aircraft for de-icing and electric actuator thermal management. He is a Member of AIAA.

Robert P. Cassoni is currently a senior in the Mechanical Engineering program at Wright State University. He graduated Summa Cum Laude in June 1996 with a B.S. degree, and will pursue a Masters degree in Mechanical Engineering at the University of Dayton. His senior design project concerns the investigation of the effects of pipe curvature on the capillary limit of a spirally grooved heat pipe. He is the School Chapter President of AIAA.

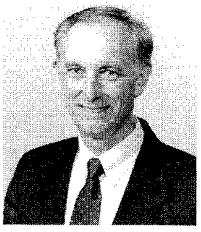

Charles MacArthur has been Chief of the Turbine Branch, Turbine Engine Division, Aero Propulsion and Power Directorate, U.S. Air Force Wright Laboratory since January of 1995. In this capacity, Dr. MacArthur also serves as the Turbine Systems Panel Chairman for the DoD-NASA Integrated High Performance Turbine Engine Technology (IHPTET) program. Previous to these assignments, he was the leader of the Wright Laboratory team that established the Air Force's Turbine Research Facility. He has been involved in gas turbine engine basic research and exploratory development since joining Wright Laboratory in 1983. Before that, Dr. MacArthur was employed by the University of Dayton Research Institute where he was involved in a number of research projects concerning aircraft safety, combustion, applied meteorology, fluid dynamics, and energy conservation. Dr. MacArthur received B.S. and M.S. degrees in Physics from the Ohio State University, and a Masters of Materials Engineering and the Ph.D. in Mechanical Engineering from the University of Dayton. He has been an adjunct engineering faculty member of the University of Dayton and Wright State University. Dr. MacArthur is the author or co-author of 23 journal articles, conference papers, and technical reports, and holds four U.S. patents.

Received Nov. 10, 1995; presented as Paper 96-0390 at the AIAA 34th Aerospace Sciences Meeting and Exhibit, Reno, NV, Jan. 15–18, 1996; revision received March 9, 1996; accepted for publication March 10, 1996.

R = radius of rotor tensile, m
R_c = recovery factor
Re = Reynolds number
r = leading-edge radius of curvature in percent of chord; radius of failure surface, m
S = surface area, m^2
s = airfoil surface arc length, m
s_l = lower limit of impingement, m
s_u = upper limit of impingement, m
T = temperature, K
t = time, s; airfoil thickness, m
t_p = pulse duration, s
V = particle velocity relative to the flowfield, m/s
V_x, V_y = components of the flowfield velocity at the droplet location, m/s
V_∞ = freestream velocity, m/s
w = transverse deflection, m
x, y = Cartesian coordinates, m
X = mass fraction
y_l = starting ordinate of the lower water droplet tangent trajectory, m
y_u = starting ordinate of the upper water droplet tangent trajectory, m
α = angle of attack, rad
α_i = induced angle of attack, rad
β = local collection efficiency
γ_c = ratio of specific heats
ΔC_d = drag increment
ΔC_l = lift increment
ΔC_m = moment increment
μ = absolute viscosity, Pa-s
ρ = density, kg/m^3
σ = tensile stress, N/m^2
τ = shear stress, N/m^2
ϕ = relative humidity
ω = angular velocity, rad/s

Subscripts

a = air
c = chord or corrected
cl = clean
cond = conduction
conv = convection
d = droplet or drag
eg = ethylene glycol
evap = evaporation
frz = freezing
i = ice
in = inlet
inc = incident
ke = kinetic energy
l = lower or lift
m = moment
max = maximum
out = outlet
sat = saturation
sur = surface
u = upper
v = vapor
visc = viscous
w = water
∞ = freestream conditions

Superscripts

$\cdot$ = first derivative with respect to time
$\cdot\cdot$ = second derivative with respect to time

I. Introduction

ICING can occur when aircraft are on the ground and in flight. On the ground, snow or freezing rain falling on the craft can result in slush, snow, clear ice, or a combination of these. Also, icing can occur on some aircraft wings while the aircraft is on the ground in ambient temperatures above freezing because of the presence of below-freezing fuel in the wing tanks. These cold spots are blamed for the crash of a McDonnell Douglas MD-81 twin jet transport operated by the Scandinavian Airlines System, according to the Swedish board of accident investigation (SHK).[1] Clear ice that formed on the wings in front of the engine air intakes came off during the takeoff roll and was ingested by the engines. Engine failure because of damage to the fan blades and compressors resulted in the downing of the aircraft within 4 min of takeoff.

In the air, icing is caused by supercooled water droplets in clouds, which are in a metastable condition. The droplets follow trajectories that will either strike the surface or will be carried away from it. When the aircraft encounters these droplets, they may either suddenly change phase upon impact, or may flow back as a thin film of water and collect into droplets because of surface tension. The droplets may be swept off the surface by aerodynamic forces or freeze. Typical atmospheric processes that result in airborne icing are discussed by Stankov and Bedard.[2] The temperature range normally associated with icing is from -40 to 0°C.

Accreted ice is normally classified as rime, glaze, or mixed. Rime ice is seen at lower temperatures (-40 to -10°C) where the supercooled water droplets freeze almost immediately onto the surface.[3] In doing so, air is entrapped between the frozen droplets, which gives rime ice its characteristic white appearance. Rime ice is normally attached to the leading edge with a streamlined shape (essentially an extension of the airfoil), where the aerodynamic drag is increased because of surface roughness and early boundary-layer transition.[4] Glaze ice occurs at higher temperatures (-18 to 0°C) where liquid droplets impact the surface, run back as a thin liquid film, and then freeze. Therefore, glaze ice is clear, with a density of $\rho = 917$ kg/m^3, whereas rime ice is less dense because of the entrapped air ($\rho = 880$ kg/m^3) (Ref. 5). If the duration of the icing encounter is sufficiently long, two glaze ice horns grow away from the stagnation point, which causes significant lift and drag penalties and may result in the inability to maintain altitude.[6,7] In a mixed ice situation, glaze ice is surrounded by delicate feather-shaped rime ice formations.[8] The type and shape of the ice formations are dependent on a variety of parameters in a complicated manner[9]: airfoil geometry, airspeed and altitude, LWC of the cloud, droplet collection efficiency of the airfoil, MVD, ambient air temperature, and cloud extent, etc.

Ice can accumulate during flight in a number of locations on the aircraft. The most critical locations are the leading edges of the wings and empennages, the propellers and hubs on fixed-wing aircraft, the engine nacelles, the rotor blades on helicopters, and the windshields. The buildup of ice on the leading edges of fixed wings causes an increase in drag, a decrease in lift, and altered moment characteristics of the aircraft.[10] Since the rotor blade of a helicopter provides thrust in addition to lift, the increased drag and torque induced by icing has a greater significance in terms of the performance requirements.[11,12] Dislodged ice can damage the aircraft skin, antennas, or other instrumentation, or can severely disable or destroy the engine if ingested. Ice shedding on helicopter blades can cause a rotating imbalance, resulting in severe vibration and control difficulties. The buildup of ice can result in the inability to retract movable surfaces, such as slats or flaps. All of these potentially severe problems point to the fact that in many situations significant icing is not permissible.

II. Methods of Airborne Anti-Icing and De-Icing

Anti-icing refers to the prevention of any buildup of ice on a surface during flight. De-icing denotes the case where ice has already formed on a surface, which is subsequently removed. Three main groups of anti-icing and de-icing methods are under current investigation or use: 1) freezing point depressants, 2) thermal melting, and 3) surface deformation. Each of these methods will be discussed in this section.

A. Freezing Point Depressants

During World War II, British aeronautical engineers developed porous leading edges that had the capability to de-ice the wings during flight. The stainless steel leading edges were provided with slots through which passed ethylene glycol.[13] After the fluid passed over the leading edge, it flowed over the aft parts of the wing, which were de-iced in the process. A fluid ice protection system used on a Cessna 206 airplane included stainless steel porous panels bonded and riveted into place over the wing leading edges, slinger rings to provide de-icing for the propeller, and spray bars to keep the windshield clear of ice.[14] A liquid pump and tank, which held 27.25 l (7.2 gal) of ethylene glycol (enough for a 3.5-h operating period) were installed in the fuselage of the airplane. The overall system added approximately 13.61 kg (30 lbm) to the empty weight of the airplane. Improvements in the leading-edge weep system include the use of sintered stainless steel fabrics and titanium laser-drilled skins having thousands of tiny holes.[15] Benefits of the glycol-exuding system include the following[16]:

1) Leading-edge airfoil contours can be retained with excellent tolerance.

2) No residual or runback ice is left on surfaces after system actuation.

3) The life of the system hardware is comparable to that of the airframe.

4) The system operates with a low power demand.

5) Little judgment is required by the pilot to operate the system safely.

Some of the system's drawbacks are as follows:

1) During de-icing, liquid systems are least effective when the adhesive bond is greatest (low LWCs, lower temperatures, and low MVDs).[17]

2) Helicopters are usually not candidates for liquid systems because of the need for long endurance times.[11]

3) Weep systems are not used in turboprop aircraft where engine bleed air is used to supply cabin air because of the possibility of producing harmful vapors in the cabin.[17]

B. Thermal Melting

Anti-icing and de-icing can be achieved by the use of thermal energy. The type of thermal melting depends on the magnitude of the heat flux delivered to the surface. High heat fluxes result in evaporative anti-icing, where the impinging liquid droplets are evaporated, which means the downstream surfaces are dry. Running wet systems denote the case in which the heat flux is lower, and the liquid droplets run back in a thin liquid film on the surface. Caution must be used in the design of such a running wet system, because of the possibility of the liquid film freezing on critical downstream surfaces (runback ice). Running wet systems are usually preferable to evaporative systems because of the significantly decreased power requirement. Typical thermal systems either use hot compressor gas, hot exhaust gas, hot oil, or electrical energy. According to military specifications, exhaust gases from turboprop or turbojet engines can only be in contact with the exhaust ducts; therefore, systems on military aircraft that reclaim exhaust waste heat must employ a heat exchanger.[18]

The most prevalent thermal anti-icing and de-icing technique is the use of hot bleed air from the high-pressure compressor of the engine (turbojet or turboprop aircraft). Alternative hot-air methods include the use of a dedicated compressor for ram air, recapturing the waste heat from the exhaust gas (piston-driven engines), and heating the ram air with a fuel-burning combustion heater. In general, the hot air is diverted from the source by interconnecting ductwork to the interior of the location to be anti-iced or de-iced (normally at the stagnation point). For wings or engine inlets, the air is discharged from the ductwork into piccolo tubes or narrow-gap passages to transfer thermal energy to the aircraft skin along the chordwise direction. The spent air is then discharged overboard through ports in the aircraft skin. The flow rate of hot air necessary for anti-icing or de-icing is dependent on the source air temperature, heat losses through the ductwork, the geometry of the piccolo tube or narrow-gap passages, as well as the same parameters that effect ice accretion, as outlined in Sec. I. Military and commercial aircraft required to operate in all-weather conditions must also provide for anti-icing of the forward-facing windshields. This is accomplished using an external air blast system that directs a stream of hot air at the bottom of the window. The airstream then flows downstream over the rest of the windshield, which forms a hot boundary layer, preventing ice buildup. In addition to anti-icing, this system also removes rain from the windshield.

Hot bleed air anti-icing is a highly reliable well-developed technology. However, with the development of future advanced engines such as geared fans (advanced ducted props), counter-rotating unducted props, and ultrahigh bypass ratio prop fans, the volumetric flow rate of the bypass air will become more significant in terms of the fuel consumption penalty.

Onboard electrical energy is used to anti-ice and de-ice by the use of electrothermal heaters where hot-air anti-icing systems are not feasible, such as propellers, spinners, nose cones, and helicopter rotors and hubs. The electrothermal pads are bonded to the outer surface in need of anti-icing. The heat generated by these electrothermal pads are conducted to the ice/surface interface, where a thin film of water is formed. This breaks the adhesive bond between the ice and the outer surface of the pad, so that the ice can be swept away by aerodynamic forces.[19] De-icing electrical power is kept to a minimum by cycling the load between the different electrothermal heaters; this helps to reduce the size and weight of the electrical generator. Bypass ducts (inertial particle separators) are used to prevent shed ice particles from being ingested by the engine. During icing conditions, some of the airflow is diverted downward away from the engine, such that the heavier-than-air ice particles are carried away from the intake.[17] A protective screen is also normally used to prevent foreign particle ingestion. Electrothermal pads are generally constructed in five layers[20]:

1) A substrate, which is usually the outer skin of the aircraft.

2) A layer of inner insulation, which is usually resin-impregnated glass cloth (needed for both thermal and electrical insulation).

3) A metallic heater element ribbon.

4) A layer of outer insulation.

5) An abrasion shield that protects the electrothermal pad from the freestream.

The main benefit of electrothermal de-icing is the simplicity of the system, and the fact that the response time is very short in comparison with hot air or hot fluid systems. However, the power consumption is very high, especially for evaporative anti-icing.

C. Surface Deformation

To reduce the amount of energy required for de-icing, surface deformation systems have been developed in which the iced surface is suddenly deformed. The ice cracks and debonds from the surface, and aerodynamic forces carry the particles away. Three main surface deformation systems have been researched: 1) pneumatic boots, 2) electromagnetic impulse de-icing (EIDI), and 3) electromagnetic expulsive boots. All of these systems may need to use inertial particle separators to prevent ice particle ingestion. In addition, surface deformation systems only de-ice, therefore, some amount of drag rise is unavoidable. A comparison of several deformation systems was made at the NASA Lewis Research Center's Icing Research Tunnel.[21]

Pneumatic boots are the most commonly used method of de-icing that employ the surface deformation technique, especially for general aviation aircraft.[17] Pneumatic boots are essentially inflatable bladders bonded to the surface to be de-iced. During

inflation, bending and shearing stresses are imposed on the accreted ice, which destroys the adhesion between the ice and the boot. The ice is typically broken into small pieces that are carried downstream by aerodynamic forces. When the boot is not pressurized, it must be evacuated to resist the negative aerodynamic pressure that could partially inflate it, which would significantly increase the drag.[11]

As with all surface deformation systems, the pneumatic boot system has a minimum ice thickness that it can eject from the surface. Current pneumatic systems can remove ice on the order of 3.175 mm (0.125 in.) and larger. Future systems will require ice-particle shed sizes as thin as 0.762 mm (0.030 in.) with equivalent particle diameters on the order of 6.35 mm (0.25 in.).[22] In fact, care must be taken in the operation of pneumatic de-icers because if the boots are used too often in glaze icing conditions, the ice can build a cap over the airspace produced by the expansion of the boots, thereby resulting in an ice formation that cannot be shed.[13]

A variation of the pneumatic boot system is the pneumatic impulse ice protection system (PIIP).[22] Instead of the relatively slow inflation of the pneumatic boot, the impulse system inflates a matrix of flat, fiber-reinforced tubes within 50 μs, which not only breaks the surface bond, but also launches the ice particles away from the surface. The system has demonstrated ice thickness shedding capabilities of 1.016 mm (0.040 in.) for dry ice conditions and 2.286 mm (0.090 in.) for slush ice. The PIIP system was analyzed for potential use on composite helicopter rotor blades by Weisend.[11]

Benefits of the pneumatic boot de-icing system include very low power requirements (as compared to electrothermal systems), low weight, and retrofittability. A major drawback is that the exact airfoil shape is not preserved since the boots are bonded onto the exterior of the airfoil.

EIDI resolves the previously mentioned problem of a nonconforming profile by actually deforming the aircraft skin. A high-amperage pulse is passed through a spirally wound, flattened coil made from ribbon wire.[17,21,23-25] The coil is rigidly supported close to the skin of the aircraft wing, but with an air gap of approximately 2.54 mm (0.1 in.). Electrical energy is discharged from a capacitor through the coil, which establishes a transient magnetic field producing eddy currents in the nonmagnetic metallic skin. The opposing magnetic fields in the coil and the skin repel each other with a force on the order of several hundred pounds, but the duration is only a fraction of a millisecond.[26] In general, two impulses of about 330 J/m are used, with a 5-s delay for recharging the capacitors.[27] The first impulse cracks and partially debonds the ice from the surface, and the second impulse launches the ice particles from the surface. If the metallic skin is too thin, it cannot provide an adequate eddy current conductance. In this case, and when composite surfaces are used for the aircraft skin, copper or aluminum disks (doublers) slightly larger than the coil (approximately 30% greater area) must be attached to the interior of the skin.[26] Since the aircraft skin is repeatedly deformed by the EIDI system, the fatigue of the skin is an important consideration. Fatigue tests were performed on two light Cessna general aviation airplane wings with the expected result that the potential for fatigue failure increases with the impulse force.[17] However, the likelihood of failure for a typical application is remote. It was recommended that fatigue testing be carried out on any new EIDI installation.

It was determined that EIDI systems used on composite wings were a source of electromagnetic interference (EMI), which was potentially dangerous with respect to the avionics systems of the aircraft.[28,29] Zumwalt[30] found that the lightning strike protection (a copper wire mesh embedded in the composite wing) was not adequate to shield the EIDI electromagnetic emissions, while emissions from an aluminum wing were within FAA standards.[28] Zieve et al.[31] tested an EIDI system and two related systems for electromagnetic compatibility: 1) the eddy current repulsion de-icing strip (EDS),[32] and 2) the eddy current repulsion de-icing boot (EDB).[33] With the EDS system, the coil and doubler are placed on the outer surface of the wing, and a titanium skin covers both to protect them from the ambient airflow. The EDB system is bonded to the exterior of the aircraft and is made of an elastomer polyurethane material. Electrically conductive ribbons are placed in the fixed portion of the boot, which is attached to the aircraft, and in the movable portion of the boot. Large opposing currents cause the movable portion to expand away from the fixed portion, thereby achieving the desired de-icing action.

III. Modeling of Icing Phenomena

To be able to determine the effects of accreted ice on the performance of aircraft and the efficacy of the previously mentioned anti-icing and de-icing techniques, models of airborne icing phenomena on aircraft have been developed. The major areas of importance in modeling icing are the flowfield around the airfoil, the trajectories of the water droplets around the airfoil, and the thermodynamic and fluid dynamic phenomena associated with the accretion of the ice on the surface.

A. Flowfield Analysis

The flowfield surrounding the airfoil can be solved using a number of methods. The following three methods have been used with success: 1) conformal mapping, 2) the panel method, and 3) the Eulerian approach. Conformal mapping was first introduced by Theodorsen[34] and Theodorsen and Garrick.[35] The two-step transformation is based on the theorem by Riemann that it is always possible to transform the potential field around any closed contour into the potential field around a circle. Once the airfoil shape is transformed into a circle, the velocities on the surface and at any point around the surface can be determined. Since this is a solution of the Laplace equation, the implicit assumptions are that the flow is both inviscid and incompressible. Bragg[36] stated that since the effects of compressibility on the water droplet trajectories were negligible up to the critical Mach number for all but the smallest droplet sizes, and the viscous effects are important only in the thin viscous boundary layer, the conformal mapping method was appropriate in solving for the accretion of rime ice on airfoils. Airfoil rime icing studies using the conformal mapping technique include those by Bragg and Gregorek[37,38] and Bragg.[39,40] Miller et al.[41] also used the conformal mapping technique to determine the flowfield around a propeller airfoil along the radial direction in rime icing conditions.

Bragg and Gregorek[37] noted that difficulties may arise in the prediction of ice shapes because of the assumption of an inviscid flowfield. When a concave surface occurs in the flowfield, a recirculation or separation bubble is formed that is not predicted by the potential flow code. The potential flow solution gives higher velocity gradients in this region, which leads to higher ice accumulation rates than those occurring in reality. This problem also leads to a limitation when the angle of attack (AOA) of the airfoil is very high.[40]

The panel method is a general solution method for the potential flow problems that describe incompressible inviscid flow. The flow can be around any two- or three-dimensional body with nearly any type of boundary condition. The panel method was developed at the Douglas Aircraft Company in the 1950s to improve the prediction of airflow around bodies of revolution.[42,43] In the panel method the surface of the airfoil is divided into a series of sections or panels that are flat in profile. In other words, the exact airfoil shape is approximated by an inscribed polygon. The panels have both source density and vorticity. Each panel may have a different source density, but the density is constant across each panel. This facilitates integration of the potential flow equations, which leads to a simple system of linear algebraic equations. For strictly potential (inviscid) flow, the source strength of each panel is iteratively determined by solving these simultaneous equations with the requirement that the total normal velocity at the sur-

face of each panel must be zero. The total normal velocity is defined as the freestream plus body sources and vortices. The vorticity strength of each panel is the same so that vorticity is defined by a total strength, which is adjusted to satisfy the Kutta condition.[44] The classical Kutta condition requires the avoidance of an infinite velocity at the trailing edge. As applied in the panel method, the Kutta condition demands that the pressures on the upper and lower surfaces approach a common value at the trailing edge.[45] Since the pressure is proportional to the square of the velocity, the Kutta condition equations are nonlinear.

Many researchers have employed the panel method code that was developed by Hess and Smith[46] (see Refs. 5–7, 43, and 47). Improvements include corrections for compressibility and the presence of a boundary layer. MacArthur[6] used the Karman–Tsien compressibility correction, whereas Hedde and Guffond[48] employed the Prandtl–Glauert correction.[49] While the Karman–Tsien correction extends the useful range of the panel method to higher Mach numbers, thick airfoils and high AOAs are not adequately predicted since the correction is based on a small perturbation approximation.[50] The same difficulty noted by Bragg and Gregorek[37] (conformal mapping technique), that is, incorrect flowfield predictions in regions of separation, was also discussed by MacArthur[6] using the panel method.

The inclusion of the viscous boundary layer can be classified as noninteractive, where the freestream does not feel the effects of the boundary layer, or interactive, where the freestream is coupled with the boundary layer. An interactive boundary-layer method was used by Refs. 44, 51–53 where the external velocity distribution was obtained from potential flow theory. A perturbation velocity resulting from viscous effects was incorporated to determine the displacement thickness iteratively. In this viscous case, the Kutta condition is applied to the displacement surface rather than on the panel surfaces. With the inclusion of the boundary layer, the effects of surface roughness and turbulence can be accounted for.

The Eulerian approach involves the construction of an orthogonal grid structure around the body. The conservation of mass, momentum, and energy equations are derived over individual control volumes fixed in space. Therefore, the changes in the properties and characteristics of the fluid are recorded as the fluid passes through the control volume.[54] The grid structure around airfoils is usually generated by solving two hyperbolic differential equations. The procedure begins on the airfoil surface, which is defined by the user, and marches outward to the far field. An orthogonal, body-oriented grid is established in which the grid points are clustered near the surface. Benefits of using the Eulerian approach include the elimination of restrictions imposed on the conformal mapping technique and the panel method for thick airfoils and high angles of attack. Also, the problems associated with concave curvatures seen with the potential flow solution methods are reduced.[50] A drawback of the Eulerian method is the necessity of interpolating the velocities between grids for use in determining particle trajectories. However, with a sufficiently fine grid, this problem can be minimized. Also, the Eulerian method is extremely costly in terms of computing resources, as compared to potential flow codes.

Scott et al.[55] used the Eulerian method to compute the flowfield around an iced cylinder. The Navier–Stokes equations were solved using MacCormack's explicit finite difference method. The effects of turbulence were accounted for at the surface by using the Baldwin–Lomax algebraic eddy–viscosity model. Potapczuk[50] employed the Eulerian method to determine the flowfield around a NACA 0012 airfoil, but the Eulerian equations were solved in body-fitted coordinates, where the viscous and heat transfer terms are dropped from the complete Navier–Stokes equations.

B. Droplet Trajectory Analysis

As previously discussed, supercooled water droplets follow trajectories that may or may not result in an impact on the surface of the airfoil. The locations of the impacts on the airfoil surface range from s_l to s_u. Similarly, the starting ordinates of these tangent trajectories are y_l and y_u, respectively. These four coordinate locations are usually found using a Lagrangian approach, where differential equations describing Newton's second law for a single droplet are solved iteratively. As opposed to the Eulerian approach, the Lagrangian methodology follows a control volume (the liquid droplet) as it passes through the region of interest. To derive the equations of motion, the following assumptions concerning the flow of water droplets in air are made[36,43,47]:

1) Because of their size ($10 \leq d \leq 50$ μm), the droplets remain spherical, and the molecular slip phenomenon is negligible.

2) The influence of the droplet on the flowfield is neglected since the LWC rarely exceeds 2.0 g/m^3.

3) The pressure gradient term, the apparent mass term, and the Bassett unsteady memory term are negligible because the droplet density is much greater than that of air.

4) The effects of the viscous boundary layer at the airfoil surface are neglected since the boundary layer at the leading edge (where most impacts occur) is very thin.

Accounting for these assumptions, the equations of motion for the droplets become

$$\begin{aligned} m\ddot{x} &= -\boldsymbol{D}\cos\gamma + mg\sin\alpha \\ m\ddot{y} &= -\boldsymbol{D}\sin\gamma - mg\cos\alpha \end{aligned} \tag{1}$$

where

$$\gamma = \tan^{-1}[(\dot{y} - V_y)/(\dot{x} - V_x)] \tag{2}$$

V_x and V_y are found as described in Sec. III.A. This form of the equations of motion is for the case when the chordline of the airfoil is perpendicular to the gravity vector and the Cartesian coordinate system is tilted along the freestream at α. The drag force $\boldsymbol{D}$ is given by Ref. 50:

$$\boldsymbol{D} = C_d(\rho_a V^2/2)A_d \tag{3}$$

where C_d is the drag coefficient of the spherical droplet, ρ_a is the density of air, and A_d is the characteristic area of the droplet. The particle velocity relative to the flowfield is

$$V = \sqrt{(\dot{x} - V_x)^2 + (\dot{y} - V_y)^2} \tag{4}$$

The flux of water that impinges on the airfoil surface is not uniform, but is usually highest at the stagnation point.[56] The mass flux on the leading edge is characterized by the nondimensional collection efficiency β. This parameter is defined as the ratio of the mass flux between two particle trajectories upstream from the airfoil to that on the airfoil surface. Assuming a constant droplet density over both locations gives

$$\beta = \frac{\mathrm{d}y}{\mathrm{d}s} \tag{5}$$

The local mass flux of water impinging on the airfoil is

$$\dot{m}''_{w,\mathrm{inc}} = V_\infty(\mathrm{LWC})\beta \tag{6}$$

The total collection efficiency of the airfoil is found by integrating the β distribution from the lower to the upper limits of impingement

$$E = \frac{1}{h}\int_{s_l}^{s_u} \beta\,\mathrm{d}s = \frac{y_u - y_l}{h} \tag{7}$$

where h is the projected height of the airfoil as seen looking

in the x direction. The total mass flow rate per unit width of water impinging on the surface is

$$\dot{m}'_{w,\text{inc}} = V_\infty(\text{LWC}) \int_{s_l}^{s_u} \beta \, ds = V_\infty(\text{LWC})(y_u - y_l) \quad (8)$$

In the derivation of Eqs. (5–8), it was assumed that the droplet diameter distribution could be adequately described by the MVD. A more general case where a multidispersed distribution is used is presented by Bragg[36] and Ruff and Berkowitz.[43] To match their flowfield velocity results, Scott et al.[55] used an Eulerian approach to determine droplet trajectories.

C. Ice Accretion Analysis

After consideration of the flowfield and droplet trajectories, thermodynamic and fluid dynamic principles may be applied to determine ice shapes and rates of ice accumulation. The phenomena that are important to this process include 1) viscous or kinetic air heating, 2) kinetic heating by water droplets, 3) evaporation or sublimation, 4) convection, 5) warming of droplets from the airfoil, and 6) heat of fusion.

To model the ice accretion, a control volume is constructed such that the upper limit coincides with the boundary layer of the airflow and the lower limit is just below the ice surface. Since the ice accumulates and changes shape with time, the position and shape of the control volume must be altered accordingly. In addition, the change in airfoil shape because of accreted ice can alter the boundary layer, thus increasing the necessary flexibility of the control volume. This idea of a transient control volume has been used by several researchers,[43,50,57] and allows all energy and mass transactions to take place at the control volume boundaries regardless of changes to the system. Once the control volume has been constructed, mass and energy balances can be applied.

As previously mentioned, the freezing characteristics of rime ice differ from those of glaze ice. To facilitate the development of general mass and energy conservation equations that can be applied to all icing phenomena a freezing fraction f was developed by Messinger[58] and is defined as the ratio of the amount of water freezing within the control volume $\dot{m}_{\text{frz}}$ to the mass flow rate of incident water droplets $\dot{m}_{\text{inc}}$, plus that of the liquid water that enters the control volume from upstream control volumes $\dot{m}_{w,\text{in}}$:

$$f = \frac{\dot{m}_{\text{frz}}}{(\dot{m}_{\text{inc}} + \dot{m}_{w,\text{in}})} \quad (9)$$

Since rime ice is characterized by water droplets freezing upon impact, the freezing fraction will be equal to unity for this case. For glaze ice, the freezing fraction will be somewhere between zero and unity. When the freezing fraction is equal to zero, the heat transfer is not sufficient to cause freezing.

The conservation of mass equation is[6,7,43,50]

$$\dot{m}_{w,\text{in}} + \dot{m}_{\text{inc}} = f(\dot{m}_{\text{inc}} + \dot{m}_{w,\text{in}}) + \dot{m}_{\text{evap}} + \dot{m}_{w,\text{out}} \quad (10)$$

where $\dot{m}_{\text{evap}}$ is the evaporative mass flow rate and $\dot{m}_{w,\text{out}}$ is the mass flow rate of liquid water out of the control volume. Accurate predictions of the flowfield, collection efficiencies, and LWC are necessary to determine the mass balances since the incident mass rate is based solely on these variables.

The conservation of energy equation is[6,7,50]

$$\dot{Q}_{w,\text{in}} + \dot{Q}_{\text{inc}} + \dot{Q}_{\text{ke}} + \dot{Q}_{\text{visc}} = \dot{Q}_{\text{evap}} + \dot{Q}_{w,\text{out}} + \dot{Q}_{\text{frz}} + \dot{Q}_{\text{conv}} + \dot{Q}_{\text{cond}} \quad (11)$$

where

$$\dot{Q}_{w,\text{in}} = \dot{m}_{w,\text{in}} c_w T_{w,\text{in}}, \qquad \dot{Q}_{\text{inc}} = \dot{m}_{\text{inc}} c_w T_\infty$$

$$\dot{Q}_{\text{ke}} = \dot{m}_{\text{inc}} \left(\frac{V_\infty^2}{2}\right), \qquad \dot{Q}_{\text{visc}} = h_c S R_c \left(\frac{V_\infty^2}{2c_a}\right)$$

$$\dot{Q}_{\text{evap}} = 0.7 h_c S h_{fg} \left[\frac{\phi P_{v,\text{sat}}(T_\infty) - P_{v,\text{sat}}(T_{\text{sur}})}{P_a c_a}\right]$$

$$\dot{Q}_{w,\text{out}} = \dot{m}_{w,\text{out}} c_w T_{w,\text{out}}, \qquad \dot{Q}_{\text{frz}} = f(\dot{m}_{\text{inc}} + \dot{m}_{w,\text{in}}) h_{sl}$$

$$\dot{Q}_{\text{conv}} = h_c S(T_{\text{sur}} - T_\infty), \qquad \dot{Q}_{\text{cond}} = S K_i \left(\frac{dT}{dn}\right)$$

$\dot{Q}_{w,\text{in}}$ is the heat rate caused by the liquid water entering the control volume from upstream, $\dot{Q}_{\text{inc}}$ is the sensible heat released by the supercooled liquid water droplets, $\dot{Q}_{\text{ke}}$ is the kinetic energy of the water droplets, $\dot{Q}_{\text{evap}}$ is the heat loss because of evaporation, $\dot{Q}_{w,\text{out}}$ is the heat flowing out of the control volume with the exiting liquid water, $\dot{Q}_{\text{frz}}$ is the heat rate because of freezing, $\dot{Q}_{\text{conv}}$ is the convective heat transfer, and $\dot{Q}_{\text{cond}}$ is the conductive heat transfer rate into the skin of the airfoil.

Recent NASA studies have revealed that surface water, especially near the impingement limits, will coalesce into beads that will remain stationary on an accreting ice surface.[57] This fact is important because these stationary beads of ice could significantly change the nature of the flowfield (and, in turn, the rate of ice accretion) in the vicinity of the beads. These same authors have proposed that two scenarios could occur. The bead could continue to grow until the freezing fraction of the bead becomes unity (complete freezing), or the bead could be removed by aerodynamic shear forces. Therefore, an investigation of the flowfield and the microphysics of the surface water are necessary for a thorough and accurate ice accretion model.

The flow behavior of water during glaze ice accretion is a function of several variables such as location on the body, surface roughness, and surface tension. The location on the body plays a role in the type of flow that is present. At the stagnation point, the flow tends to be more like a thin film. Near the impingement limits, the water separates into streams or rivulets of flowback water.[57,59] Between these two extremes, a rough zone exists in which the water coalesces into stationary beads. Pais et al.[60] found that the location on the body significantly affects the convective heat transfer. In areas of surface discontinuity such as ice horn tips high rates of convective heat transfer were observed. Also, it was found that the convective heat transfer increased on the low-pressure side of the body relative to the high-pressure side when the AOA was increased. The surface roughness can control the convective heat transfer by tripping the laminar boundary layer. Once the flow becomes turbulent, the heat transfer becomes dependent upon the surface roughness and can increase significantly, which can determine whether the water will run back or be frozen at the point of impingement. There are several empirical models that deal with surface roughness.[44,51,52] The surface roughness also affects the contact angle hysteresis of the water drops, which is related to surface tension. The surface tension causes the fluid to minimize its surface area, causing beads to be formed. The contact angle is the angle that the liquid–vapor interface makes with the solid surface on which the liquid rests. Contact angle hysteresis is the difference between the angles associated with the leading edge of the drop and that of the trailing edge. As the contact angle and contact angle hysteresis increase, the resistance to motion tends to increase.[57]

Viscous effects play a major role in the determination of ice accretion, especially in cases of flow separation such as high AOAs and major surface irregularities (ice horns). Yamaguchi

and Hansman[61] compared ice accretion models of iced cylinders with viscous as well as inviscid flowfields to experimental data. The results showed that a viscous flowfield consideration greatly increased the accuracy of the ice accretion model, particularly in areas of flow separation and recirculation. Cebeci et al.[51] found that at higher AOAs and longer time intervals, a viscous flowfield consideration predicted accreted ice shapes more accurately. It is likely that the use of a viscous flowfield will have a more pronounced effect on accuracy with improvements in the heat transfer modeling.

Since knowledge of $\dot{m}_{w,\text{in}}$ is necessary to calculate the freezing fraction and thus the mass and energy balances for each control volume, it is necessary to start the solution of the accreted ice at the stagnation point of the body where it is assumed that there is no runback water.[50] Elimination of this parameter allows a solution for an initial control volume and therefore the solution for consecutive downstream control volumes. An initial surface roughness must be assumed as well as a method to compute new surface roughnesses as ice accumulates. MacArthur[6] proposed that the surface roughness of a new layer of ice is influenced by the roughness of the old surface as well as the rate at which the ice had accumulated. This is supported by the fact that the smooth to rough zone tends to migrate towards the stagnation point with time. Since the surface roughness is changing with respect to time, consideration of the transient nature of the location of the laminar-to-turbulent transition point is necessary.

Although the ice accretion analysis up to this point has only considered a two-dimensional flowfield, the mass and energy balances are readily expandable to a three-dimensional treatment. A three-dimensional analysis has the advantage of modeling swept wing aircraft and other surfaces that two-dimensional analyses cannot model accurately.[48] To implement a three-dimensional analysis, two-dimensional considerations of the runback water are necessary. Because of transverse pressure gradients on three-dimensional airfoils, the streamlines at the top of the boundary layer may have a direction up to 20 deg different than at the bottom. Hedde and Guffond[48] found it necessary to use the wall streamline trajectory to calculate the runback directions for fully three-dimensional objects. However, for swept wings the results were independent of the source of the runback directions.

D. Performance Degradation

Ice accretion on aircraft has been investigated a great deal over the past few decades because of the detrimental effects that it has on aircraft performance. With airfoils, these effects include decreased lift, increased drag, and instability caused by adverse moments. With propellers, ice accretion can decrease thrust. Any one of the previous situations could have disastrous consequences. It is therefore necessary to understand the performance degradation caused by ice accretion as well as to investigate methods to model it.

The performance degradation caused by glaze and rime ice accretions differs significantly. This can be understood by observing the differences in form and texture between the two. Therefore, the performance degradation of each ice type will be considered separately.

Glaze ice, which in severe cases is characterized by large ice horn formations near the leading edge, causes large increases in drag and decreases in the maximum lift coefficient because of flow separation behind these formations.[62] A shift in the zero-lift AOA is observed, but is not as severe as in the case of rime ice accretions. This is caused by the rougher surface on the rime ice accretion near the stagnation point that results in a thicker upper surface boundary layer near the leading edge than on the glaze ice accretion. Although glaze ice accretions increase the surface roughness over the clean airfoil, the shape has a much more significant effect on performance degradation. For this reason, performance degradation of glaze ice horns can be modeled without consideration of surface roughness effects with nearly the same accuracy, especially for maximum lift and drag. In addition to the lift and drag degradation, Ranaudo et al.[10] found that glaze ice accretions on horizontal tail sections resulted in an inhibited elevator effectiveness that resulted in decreased sensitivity of the aircraft to elevator control inputs, especially at low speeds.

Rime ice, which is characterized by a rougher surface near the stagnation point and more streamlined appearance, causes a smaller increase in drag than glaze ice horns. Since rime ice accretions retain the streamlined appearance of the airfoil, the surface roughness which causes premature boundary-layer transition is the primary cause of increased drag.[62] The leading-edge surface roughness also causes a decrease in the maximum lift coefficient and shift in the zero-lift AOA as discussed earlier.

Methods of measuring performance degradation by using simulated leading-edge ice shapes for wind tunnel or actual flight testing are presented.[5,10,37,44,62,63] In addition to the simulated ice shapes, Bragg et al.[62] investigated several other experimental methods to simulate glaze and rime ice performance degradation. Various levels of simulated surface roughness were tested that were particularly useful in the measurement of performance degradation because of rime ice accretions. Also presented were oil flow experiments on glaze ice accretions to determine the length of flow separation aft of the horn formations. Khodadoust and Bragg[63] presented several methods of determining flow patterns of iced airfoils in both normal and swept configurations. The experimental methods that included oil flow and helium bubble flow visualization techniques showed promising agreement with Navier–Stokes calculations.

Although experimental modeling of an iced airfoil (simulated or real) is a reliable method to measure performance degradation, the availability of sufficient testing facilities, airfoil shapes, as well as different ice shapes can prove to be cumbersome and expensive. Therefore, many empirical correlations for performance degradation have been developed. Empirical correlations to measure changes in lift and drag coefficients caused from ice accretions have been developed.[36,64,65] Gray[64] gives the following correlation for the drag increment for rime and glaze ice:

$$\Delta C_d = \left[\left[(8.7 \times 10^{-5})\frac{t_i V_\infty}{c}\sqrt{\text{LWC}\,\beta_{\max}}\,(32 - T_\infty)^{0.3}\right] \times \left(1 + 6\left\{(1 + 2.52r^{0.1}\sin^4 12\alpha) \times \sin^2\left[543\sqrt{\text{LWC}}\left(\frac{E}{32 - T_\infty}\right)^{1/3} - 81 + 65.3\left(\frac{1}{1.35^{\alpha_i}} - \frac{1}{1.35^{\alpha}}\right)\right] - \frac{0.17}{r}\sin^4 11\alpha\right\}\right)\right] \Big/ C_{d,\text{cl}} \tag{12}$$

where t_i is the icing time, r is the leading-edge radius of curvature in percent chord, c is the chord length, α_i is the induced AOA, and $C_{d,\text{cl}}$ is the clean airfoil drag coefficient.

Bragg[36] developed the following drag correlation for use on rime-iced airfoil sections:

$$\Delta C_d = 0.01[15.8\,\ell n(k/c) + 28{,}000A_c E + I] \tag{13}$$

$$A_c = V_\infty t_i\,\text{LWC}/\rho_i c \tag{14}$$

I varies according to the airfoil.

Flemming and Lednicer[65] developed the following correla-

tions that model drag, lift, and moment characteristics of iced airfoils. For glaze ice

$$\Delta C_d = \{KD_1[0.00686K_0(t/c)^{1.5}(\alpha + 6) - 0.0313(r/c)^2 + 0.006KDM^{2.4}] \times [\mathrm{LWC}(c/0.1524)^{0.2}\gamma_c(c/0.1524)^{-1.2}]\}/C_{d,\mathrm{cl}} \quad (15)$$

For rime ice

$$\Delta C_d = [0.158\ \ell n(k/c) + 175(V_\infty/\rho_i c)\mathrm{LWC}\ t_{i,c} + 1.70] \times [(\alpha + 6)/10] \quad (16)$$

For glaze and rime ice accretions

$$\Delta C_l = (KL\{-0.01335K_0(t/c)[\alpha + 2 + 0.00555KL_1(\alpha - 6)^2]\} \times [\mathrm{LWC}(c/0.1524)^{0.2}t_{i,c}(c/0.1524)^{-1.2}])/C_{l,cl} \quad (17)$$

$$\Delta C_m = \{[(0.00179 - 0.0045M)0.000544K_0\alpha(t/c)^{-2.7} + 0.00383M(1 - 63.29r/c)] \times [\mathrm{LWC}(c/0.1524)^{0.2}t_{i,c}(c/0.1524)^{-1.2}]\}/C_{m,\mathrm{cl}} \quad (18)$$

$$K_0 = K(1 + 0.0967Re_d^{0.6397}) \quad (19)$$

where K is the inertia parameter

$$K = \frac{\rho_d\, \mathrm{d}V_\infty}{18c\mu} \quad (20)$$

KD_1, KD, KL_1, and KL are functions of temperature and AOA, Re_d is the droplet Reynolds number, t is the airfoil thickness, and $t_{i,c}$ is the corrected icing time.

The previous correlations represent degradation ratios rather than increments. It is therefore necessary to use the following relation to determine the drag, lift, and moment coefficients in the iced condition:

$$C_{j,i} = (1 + \Delta C_j)C_{j,\mathrm{cl}}, \qquad j = d, l, m \quad (21)$$

The Bragg[36] and Gray[64] correlations tend to overpredict the drag performance degradation, whereas the Flemming and Lednicer[65] correlations underpredict the iced coefficient ratios. The Flemming and Lednicer correlations [Eqs. (15–18)], which have been developed for rotorcraft airfoils, have the ability to calculate ice shedding, however, the radial icing extent tends to be overpredicted leading to an overprediction of performance degradation. Overall, Bragg's correlation [Eq. (13)] produces the most reasonable drag coefficients, but is limited to rime ice accretions.

Many researchers have successfully used the previous correlations in conjunction with numerical calculations of the flowfield to determine the icing characteristics of particular airfoils. Miller et al.[41] presented a method of measuring performance degradation of propellers caused by various levels of ice accretion. Using the Theodorsen method, an inviscid flowfield was calculated at specified radial locations. After the flowfield was defined, empirical correlations[36,64,65] were used to measure changes in lift and drag coefficients. Because of the high degree of radial icing extent in helicopter rotor situations, the determination of the rime-to-glaze ice transition point would improve the results in these specialized cases.

Bragg and Gregoreck[37] presented a more numerically intensive approach to the modeling of performance degradation because of rime ice accretion on an airfoil. This method, which assumed an inviscid, incompressible flowfield, accounted for the ice shape and lift performance degradation numerically using computer codes[66,67] while it relied on an empirical correlation to determine the drag. Bragg et al.[62] extended this method by numerically determining the degradation caused by surface roughness. Although the method was unable to model the performance degradation caused by glaze ice accretion, the separation length aft of the horn formations was determined for different glaze ice shapes using the potential flow code of Bristow.[68] The calculated results showed promising correlation with the separation determined by oil flow experiments.

Griffiths and Korkan[5] presented a method very similar to that of Bragg and Gregoreck.[37] While the method showed inconsistencies in its prediction of lift and drag coefficients, it successfully merged LEWICE to the airfoil characteristic determination code of Eppler and Somers.[67]

Although glaze ice horns result in more serious penalties, most of the numerical models presented up to this point have been limited to the consideration of performance degradation because of rime ice accretions. This has been largely from the constraints imposed by available computer resources. As mentioned earlier in this section, large separation bubbles form aft of the horn formations. To accurately model the flowfield in these complicated regions, it is necessary to involve a Eulerian approach[50] or an interactive boundary layer method.[44,51,52]

The interactive boundary-layer approach was used to measure the performance degradation caused by various levels of ice accretion and surface roughness.[44,51,52] To accommodate the complicated ice shapes, two methods were employed to reduce the sensitivity of the calculations caused by the accreted ice. The first consists of a continuation method in which the ice is gradually introduced into the calculations. The solution starts with a clean airfoil for $\alpha = 0$ deg. The interactive boundary-layer method is then introduced until convergence is reached. The ice shape is then incorporated by using incremental values of the ice thickness while iterating for convergence during each step. For other AOAs, the pressure distribution is calculated from the blowing velocity at the previous AOA and then the process is repeated. The second method begins by treating the iced airfoil as a smooth surface by covering the leading-edge region. The process is very similar to the first method except that the iterations move from the smooth surface to the iced surface. The results showed a good agreement with experiments up to an AOA of $\alpha = 5$ deg in the measurement of lift, drag, and pressure distribution. Profiles of the upper surface mean velocities for an iced NACA 0012 airfoil using the second method described previously were presented.[44] The calculated velocity profiles agreed well with experiments outside the region of separation, but showed significant discrepancies within the region. Cebeci et al.[51] extended this method by incorporating the interactive boundary-layer method into LEWICE to predict the accreted ice shapes and resulting performance degradation. This method, which featured a hands-off smoothing technique, solved the problems associated with multiple stagnation points as well as reduced computer times by around 65% over the standard LEWICE code. Shin et al.[52] extended the method of Cebeci et al.[51] by studying the effects that airspeed, temperature, droplet size, LWC, and AOA have on accreted ice shapes and the associated drag. The results were consistent with experimental results, especially in rime ice accretions up to stalling AOAs.

IV. Modeling of Anti-Icing and De-Icing Methods

Having described the existing mathematical models of the physical phenomena involved during ice accretion, attention is now turned to the modeling of the three methods of airborne anti-icing and de-icing: 1) freezing point depressants, 2) thermal melting, and 3) surface deformation. The most current models are presented, where the aim is to provide direction for future efforts.

A. Freezing Point Depressants

To elucidate the pertinent physical phenomena involved in the de-icing process using freezing point depressants, the ex-

perimental study conducted by Kohlman et al.[16] will be discussed. A wing section taken from a single-engine airplane was mounted vertically in the NASA Lewis Research Center's Icing Research Tunnel. A weep system was installed onto the wing section such that fluid was delivered to three separate subsections: 1) above, 2) below, and 3) at the center of the chord. The three individual weep sections could be activated independently. In general, fluid ice protection systems can be operated in three different modes depending upon the icing condition and exposure time. The normal operation of the system is in the anti-ice mode in which the glycol flow rate is sufficient to prevent any ice from forming. The natural de-ice mode occurs when the glycol flow rate is below that of anti-icing, but still considerable enough that no permanent ice accretions will form. In the de-ice mode, the flow rate is adjusted such that it is sufficient to shed ice accretions that are formed prior to system operation.

Kohlman et al.[16] investigated the minimum fluid (80% monoethylene glycol, 20% de-ionized water) flow rates necessary to achieve the different modes of system operation for a variety of icing conditions. The method of determining the anti-ice threshold flow rate consisted of the following steps. At a given flight condition, the flow rate was set well above the anti-ice threshold flow rate using only the upper and lower sections of the fluid ice protection system. The flow rate was then reduced in steps, allowing about 30 s for system stabilization between each step, until small flecks of ice began to appear near the stagnation point. These small flecks would then be swept downstream after a few seconds. The effects of a variety of icing conditions were investigated. In general, the required flow rates increased as LWC and airspeed increased, and as temperature decreased. The threshold flow rate was not significantly affected by the AOA as long as the stagnation point was not too close to the edge of the porous skin.

To determine the natural de-ice flow rate, the flow rate was adjusted to allow the formation of continuous spanwise bars (3–7 mm thick and 5–10 mm wide) of ice along the stagnation line, which would shed in intervals of 2–7 min using only the center section of the fluid ice protection system. In general, the LWC, airspeed, temperature, and AOA tended to affect the natural de-ice mode in a similar manner to that of the anti-ice mode. The natural de-ice threshold flow rates were substantially lower than those for anti-icing, often as low as 25–50% of the anti-ice threshold flow rates.

To determine the de-ice threshold flow rate, the flow rate was set at a level greater than or equal to that required for anti-icing, using only the upper and lower sections of the fluid ice protection system to prevent the ends of ice caps to adhere to an unprotected portion of the leading edge. At each test condition, the icing spray was turned on for a specific period of time and then turned off. Next, the center section of the fluid ice protection system was adjusted to a particular flow rate to determine the time required to shed the leading-edge ice cap. The time required for de-icing decreased as the flow rate was increased, although adequate ice shedding times were achieved with anti-icing flow rates. At α = 7.8 deg, the de-icing times were as low as half of those required at α = 1.2 deg. However, the stagnation point should not approach the edge of the active porous region. Interestingly, the times required to shed ice accretions formed at −15°C were lower than for those formed at −3.9°C. The reason is that glaze ice, which attaches more securely to the leading edge, is formed at the higher temperature.

Although wind-tunnel testing is a reliable and accurate method of determining the flow rates necessary for anti-icing, the use of empirical and analytical methods could be more practical. Albright[15] and Kohlman and Albright[56] presented a semianalytical method for determining the glycol flow rate necessary for anti-icing. This method assumes that the minimum flow rate of ethylene glycol necessary for anti-icing at the location of the maximum impingement efficiency results in a freezing temperature between ambient and total temperature. This temperature is an arbitrary, empirical assumption used for velocities less than or equal to 90 m/s. The following steps outline the procedure:

1) Calculate the maximum local collection efficiency β_{max} as shown in Sec. III.B.

2) Calculate the rate of water impingement per unit area using the following equation:

$$\dot{m}''_{w,inc} = 0.0031\beta_{max}V_\infty(\mathrm{LWC}) \tag{22}$$

3) Determine the ethylene glycol mass fraction X_{eg} required to produce a freezing temperature equal to the average between the ambient and stagnation temperatures.

4) Calculate the ethylene glycol mass flow rate per unit area required to achieve X_{eg} given the water catch rate using the equation

$$\dot{m}''_{eg} = \frac{X_{eg}\dot{m}''_{w,inc}}{X_{eg,in} - X_{eg}} \tag{23}$$

where $X_{eg,in}$ is the mass fraction of the ethylene glycol being exuded from the porous section.

While simplistic, this method was successful in providing a reasonable prediction of the anti-icing mass flow rates of the ethylene glycol in comparison to the experimental values.

B. Thermal Melting

Researchers investigating the mathematical modeling of de-icing have concentrated primarily on the performance of electrothermal de-icing pads.[19,20,69–76] Only one work on modeling hot air anti-icing systems appears to have been reported.[77] The research on electrothermal pads seeks solutions to the transient conduction problem in the composite structure made of the ice layer and the airfoil structure containing the heater elements. Prediction of melting and shedding is the primary objective, and progressively more sophisticated methods have been developed over the last several years. Some of the electrothermal pad models have been coupled with ice accumulation codes to predict both the growth and shedding phenomena. In contrast, the paper by Al-Khalil et al.[77] assumes the metal skin surface (of an engine nacelle in this case) to be heated above freezing by hot engine air. Energy balances are performed on the collecting water layer to determine what level and distribution of heating is needed to prevent freezing.

The first reported effort on the detailed modeling of electrothermal de-icing is that of Keith et al.[69] and Wright et al.,[70] who compared different geometric formulations and numerical methods for solving the transient heat conduction problem in modeling the composite structure comprised of the ice layer, abrasion shield, heater, and insulation layers. Keith et al. compared the accuracy of three methods of representing the ice–airfoil surface geometry: a simple one-dimensional representation; a planar two-dimensional model that incorporates lateral conduction effects; and a coordinate transformed, or mapped, two-dimensional model that allows for airfoil surface curvature. The heat conduction equation for each method was solved by finite difference techniques. Not surprisingly, the two-dimensional models were found superior to the one-dimensional model. Further, the two-dimensional mapping treatment was superior when strong curvature affected the lateral conduction.

The key element in modeling the physics of the problem is prediction of the regions of melting, especially in a computationally efficient manner. Most models, including those of Keith et al. use what has been termed the method of assumed states (MOAS) to efficiently predict the location of the phase-change interface.[78,79] MOAS eliminates the need to iteratively solve the energy conservation equation, written in terms of enthalpy, to find the phase at each solution node. Instead, the latent heat of the ice–water phase change is replaced by a

fictitious, very large heat capacity assigned over a very small temperature range. This results in three unique, separate linear relationships between the enthalpy and temperature over the three states of the problem: ice, liquid water, and the ice–water equilibrium mixture (the mushy region). In the numerical solution procedure, a phase is assumed at each solution point, new temperatures are calculated at each point from the discretized energy equation written in terms of temperature, and the phase at the solution point is then updated based on the new temperature and temperature–enthalpy relation of each phase. In practice, it has been found that some additional transition rules must be applied to the operation of selecting the phase at each node to make the simulation more realistic. Nevertheless, the performance of models based on MOAS is sufficiently accurate to have become widely used for the melting simulation.

Even with the advantages offered by MOAS, the simulation of the heating and melting processes requires considerable computer time and thus there is a need to identify the most computationally efficient numerical techniques. By comparing nine separate finite difference numerical techniques, Wright et al.[70] showed that the direct solution of the unsteady heat conduction equation in a two-dimensional problem by the alternating direction implicit (ADI) procedure was the most economical. An increase in speed of about 25-fold over the simple explicit solution was achieved. Wright et al. also evaluated their ADI-based model for numerical accuracy and compared the results to experimental data on the de-icing of a helicopter blade.

A more complete two-dimensional model of electrothermal de-icing was reported by Henry.[71] The treatment of the physics of the conduction problem employed the MOAS approximation, but in addition both accretion and shedding of ice were included. A simplified staircase model of the ice shape discretized the ice into cells that can grow in thickness to represent the accretion. Runback water is also accounted for by staircase control volumes whose mass is determined from continuity and a few ad hoc assumptions about the dynamics of the runback. Henry's model also contains a finite difference boundary-layer code for the calculation of the convective heat transfer rate at the air–ice interface. For ice shedding, two criteria involving the calculated dimensions of the ice and water layers are used to identify which ice cells are shed. Henry compared the performance of the model in both de-icing and anti-icing situations vs data on a helicopter blade in an icing wind tunnel.

In a paper appearing at the same time as that of Henry,[71] Wright et al.[73] also reported a two-dimensional model that included accretion and shedding. Accretion was computed with the LEWICE code,[6,43] while shedding was modeled by considering the aerodynamic and centrifugal forces on the ice layer (the centrifugal force appearing in the case of icing on propellers or helicopter rotors). Empirical data were used to characterize the ice-to-subsurface bond strength as a function of temperature. Ice was assumed to be shed when the net average (over a complete spanwise section) of the shedding forces exceeded the net average bonding force. The authors demonstrated the operation of the model in a number of typical de-icing situations.

Yaslik et al.[19] continued the development of more sophisticated modeling of electrothermal de-icing systems with a three-dimensional transient conduction and melting model. The model incorporated many of the same assumptions and techniques of the earlier one- and two-dimensional codes, but did not incorporate a complete ice accretion calculation. Instead, the user can input an assumed rate of accretion. Testing of the three-dimensional model was performed using data on a horizontal stabilizer section in the NASA Lewis Research Center's Icing Research Tunnel. Results showed that the numerically predicted shedding time agreed reasonably well with the icing tunnel results.

Another significant model validation exercise of anti-icing and de-icing models was reported by Fanelli et al.[20] One- and two-dimensional ice-substrate models were evaluated vs data taken in the B. F. Goodrich Icing Wind Tunnel. The two-dimensional model was combined with the LEWICE accretion code. Both de-icing and anti-icing cases were examined. Testing was performed on a NACA 0012 airfoil section with a 13-element leading-edge electrothermal pad.

Much of the difficulty of faithfully modeling de-icing, anti-icing, and even just ice accumulation lies in the accurate representation of the true three-dimensional geometry of the problem. Finite difference numerical solution methods are generally numerically efficient, but are difficult to apply to irregular two- and three-dimensional shapes because of mismatches between the grid system and the surface boundaries. The finite element method (FEM) for the solution of the conservation equations has evolved as a technique that is markedly superior in the treatment of complicated geometries. A finite element formulation and solution of electrothermal de-icing has been developed by Huang et al.[74–76] The FEM model uses the MOAS for efficient treatment of the phase-change boundary tracking. Further efficiencies in computation are achieved by assuming a constant thermal conductivity in the two-phase region and applying LU decomposition in the matrix solution. Huang et al. applied the three-dimensional FEM model to study the effects of wing surface curvature, heater geometries, wing sweep, and the wing fuselage intersection on de-icing performance.

In contrast to the relatively numerous works on the modeling of electrothermal de-icers, published work on hot air de-icing/anti-icing apparently has been confined to a paper by Al-Khalil et al.[77] These authors constructed a three-dimensional water droplet accumulation and water runback model for the inlet cowl and nacelle of a turbofan engine installation. The objective was to study the temperature distribution of the skin and water and to evaluate operating parameters necessary to keep the incident water from freezing. It was found that directing most of the hot air to the stagnation line on the cowl leading edge worked best in maintaining liquid runback.

C. Surface Deformation

As mentioned in Sec. II.C, surface deformation methods present an efficient (low-energy requirement) method of ice removal. This is because of the impulsive nature (EIDI and PIIP) of these devices that deliver high amounts of energy over short time intervals as well as their discrete operation. Investigation of the physics involved in surface deformation methods and ice shedding are necessary to optimize current systems.

EIDI uses a high-amperage pulse through a spirally wound coil to create an impulse in the aircraft skin. Investigation of the strength of this impulse has been modeled by several researchers. The impulse strength of EIDI systems experimentally using ballistic pendulums or other experimental methods has been investigated.[26,80,81] Schrag and Zumwalt[26] presented the dependence of impulse strength on plate material and thickness, number of coil turns, coil-to-target separation, and circuit capacitance. Lewis[80] presented a similar work that investigated the dependence of impulse strength on plate conductivity, coil-to-target separation, plate thickness, and discharge frequency. These researchers also presented design criteria for EIDI design. Bernhart and Schrag[81] investigated the effect that a transient gap separation would have on EIDI operation by using a stationary coil and a mechanically oscillated target.

Analytical models of the electrodynamic phenomena involved in EIDI systems have also been presented.[32,80–82] Zieve[82] presented the design and analysis of a low-voltage EIDI system, whereas Smith and Zieve[32] presented the design and analysis of EDB and EDS systems. Bernhart and Schrag[81] presented a model of the basic EIDI system in which equations describing the electrical circuit and the magnetic behavior of

the coil and target were derived. The circuit, coil, and target equations were solved simultaneously to determine the currents in the various coil segments and target elements. Using this solution, the normal force on each target element was expressed in terms of the magnetic flux density at each element. With this result, the normal pressure on the target and the radial force through the target were found.

The dynamic response associated with EIDI impulses were investigated.[24,27,83] Gien[24] demonstrated the response on a thin circular plate and a thin semicylindrical shell using experimental and finite element techniques. The experimental and analytical results agreed well in the measurement of acceleration and displacement at discrete points, although sensitivity to spurious flexural waves resulting from the spatial discretization of the structures was shown to be significant. Scavuzzo et al.[83] used finite element modeling to predict the dynamic response of an airfoil coated with rime ice. Analytically determined impulse forces of an EIDI system were used as input to the finite element model. Separate plate elements representing an aluminum skin and a layer of accreted rime ice were connected by weightless stiff beam elements to provide the shear connection between the plate elements. The displacement results were compared to experimental results using holographic images. Bernhart and Zumwalt[27] presented an analytical model of the dynamic response of a flat rectangular plate (simply supported on all sides) to electroimpulse-type de-icing forces. The plate response is governed by the differential equation

$$D\nabla^4 w + \rho H_p \frac{\partial^2 w}{\partial t^2} = q(x, y, t) \tag{24}$$

where D is the flexural stiffness, $w(x, y, t)$ is the transverse deflection, ∇^4 is the biharmonic differential operator, and $q(x, y, t)$ is the prescribed normal pressure distribution. It is important to note that this model is limited to small deflections on completely simply supported rectangular plates. The normal deflection can be expressed as

$$w(x, y) = \sin(m\pi x/a)\sin(n\pi y/b) \tag{25}$$

where a and b are the rectangular dimensions of the plate and m and n are modal integer values. This equation satisfies both geometric and natural boundary conditions with the free vibration natural frequencies expressed as

$$\omega_{mn} = \pi^2[(m/a)^2 + (n/b)^2]\sqrt{(D/\rho H_p)} \tag{26}$$

The model presented assumed that the de-icing forces are independent of the motion of the plate. This assumption is justified by the short impulse duration (150–350 μs) characteristic of EIDI systems. The prescribed normal pressure distribution may be further expressed as

$$q(x, y, t) = p(x, y)\varepsilon(t) \tag{27}$$

where

$$\varepsilon(t) = \sin(\pi t/t_p) \qquad (t \leq t_p) \tag{28}$$

where t_p is modeled by a half-sine wave and $p(x, y)$ is the spatial pressure distribution and is dependent on structural and electrical parameters such as plate thickness, coil-to-plate gap, plate conductivity, coil geometry, and the voltage and capacitance of the discharge circuit.

Aerodynamic and centrifugal forces often play a role in the removal of ice from aircraft surfaces. Scavuzzo et al.[12] investigated the effect that centrifugal forces have in the removal of ice on rotating airfoils. Finite element modeling was used to study the tensile and shear stresses at the ice–airfoil interface. In the study, two models were developed. The first was a simple rotating beam-ice structure that showed that the shear stresses increased linearly with the ice thickness while the tensile stresses approached zero for a fully bonded surface. When the local shear stresses exceed the strength of the bond, adhesive failure occurs and tensile stresses develop in these regions. These stresses can be expressed as

$$\tau = \frac{H_i\omega\rho(R^2\omega^2\rho - 2\sigma)}{\omega\rho R + \sqrt{2\rho\sigma}} \tag{29}$$

$$\sigma = \frac{\omega^2\rho(R - r)^2}{2} \tag{30}$$

where r is the location of the failure surface. The second part of the study modeled the OH-58 helicopter tail rotor with a measured ice profile. The results were compared to icing wind-tunnel results under similar conditions. The results (probability of ice shed) agreed favorably with the experimental results when finite element uncertainty was considered.

Scavuzzo et al.[84] presented a study on the influence of aerodynamic forces in the shedding of accreted ice using finite element analysis. A two-dimensional Navier–Stokes numerical treatment was used to determine the flowfield characteristics and pressure coefficients around the iced airfoil. The pressure distribution around the ice profile could then be determined from the relationship

$$P = \tfrac{1}{2}C_p\rho_a V_\infty^2 \tag{31}$$

The stresses caused by aerodynamic shedding forces at air velocities less than $M = 0.45$ were found to be insignificant. However, at $M = 0.60$, the maximum induced shear stress was found to be 20% of the shear debonding strength.

V. Conclusions and Recommendations

A survey of airborne de-icing and anti-icing techniques is presented in this paper. In addition, the most recent models of the various phenomena occurring throughout the icing and de-icing processes are given. While great strides have been taken toward the solution of the icing problem, further work is needed for improvement of predictions and the methods of removing ice from aircraft. Alternate methods of airborne anti-icing and de-icing may include devices that can use a portion of the vast amount of available waste heat from the engines for de-icing purposes. For example, a passive two-phase heat transfer device such as a heat pipe could be employed to transfer heat from the engine to the location in need of de-icing with no performance penalties. This is because of the fact that heat pipes use a portion of the transferred heat to drive the system, therefore, an external power supply is not required.[85] Other sources of waste heat could also be used, such as power electronics or electrical actuators that are proposed in the More Electric Aircraft Initiative.[86] In addition to heat pipes, the use of combined technologies can be exploited, such as an EIDI system with integral heaters. By applying a small amount of heat to the iced location prior to activating the EIDI system, the amount of power input to the EIDI system could be reduced while increasing its efficacy. In addition, the residual ice that is normally left by the EIDI system could be completely eliminated by the electrical heaters. The power requirements for such a device would be much less than a traditional electrothermal system, but would have the potential to operate more effectively than a stand-alone EIDI system.

While the accretion of rime ice on airfoils seems to have been solved satisfactorily, glaze ice accretion and the accompanying behavior of runback ice continue to be difficult problems to solve. For this type of analysis, the interactive boundary-layer method will probably continue to be the dominant solution procedure in the near future. At some point, however,

the solution of the complete Navier–Stokes equations for the transient icing phenomenon will become tractable as the speed and capabilities of computing machines continue to increase. Many codes are currently available for the solution of such problems, but the computing cost is quite high. Eventually, a fully three-dimensional solution will be attainable, which could significantly improve predictions from the complex three-dimensional flowfield surrounding even a straight wing section. For the present, improvements in the interactive boundary-layer methods can be made by further analysis of the significance of the small-scale phenomena intrinsic to airborne icing, such as the surface roughness of the ice and the resulting convective heat transfer because of surface roughness. In fact, the amount of experimental data available for the description of the heat transfer characteristics of an iced surface is small, in spite of the fact that it is a significant factor with respect to glaze ice accretion. Experimental analyses of the effects of surface tension and contact angle hysteresis should also be made with respect to the convective heat transfer because of the importance of stationary beads of runback ice. A better understanding of the relationships between the characteristics of the droplet trajectory within a separation bubble aft of an ice horn is critical to the analysis of glaze ice formation. The accretion of ice on the horizontal stabilizers should also be investigated in greater detail with respect to the moment characteristics of the aircraft. Since the passage of the wing through the airspace ahead of the stabs results in a relatively dry wake (lower LWC), the accretion of ice will be quite different on those surfaces.

It appears that the most effective methodology for analyzing the de-icing of aircraft structures using electrothermal pads will continue to be the FEM coupled with the method of assumed states. The FEM allows for the irregular body-fitted coordinates necessary to model not only the surface of the structure, but also the surface of the ice. To fully model the electrothermal de-icing process, a complete coupling of the flowfield, ice accretion process, and surface of the iced portion must be made. In the near term, this can be accomplished by iteratively using the results of a finite difference code for the flowfield as inputs to the FEM code for the electrothermal pad and airfoil skin. This linking will require improvements in the ability to match the grid structures between the two codes, which is not an insignificant problem. The same type of matching between the flowfield and the airfoil surface is also needed for the analysis of EIDI systems. Improvements in the models of EIDI systems are needed concerning the boundary conditions. For example, a simply supported rectangular plate probably does not accurately reflect the physics involved in the skin of an aircraft that is riveted to the supporting structures.

Acknowledgments

This work was initiated by S.K.T. under the auspices of a NASA–ASEE Summer Faculty Fellowship Program at NASA Lewis Research Center. Additional funding was provided by the Ohio Board of Regents under Ohio Research Initiation Grant No. 662143.

References

[1]Sparaco, P., "Swedish Crash Prompts Clear-Ice Guidelines," *Aviation Week & Space Technology*, Jan. 10, 1994, pp. 49, 50.

[2]Stankov, B., and Bedard, A., Jr., "Remote Sensing Observations of Winter Aircraft Icing Conditions: A Case Study," *Journal of Aircraft*, Vol. 31, No. 1, 1994, pp. 79–89.

[3]Heinrich, A., et al., *Aircraft Icing Handbook*, FAA Technical Center Publication, Atlantic City, NJ, 1991.

[4]Bragg, M., Gregorek, G., and Lee, J., "Airfoil Aerodynamics in Icing Conditions," *Journal of Aircraft*, Vol. 23, No. 1, 1986, pp. 76–81.

[5]Griffiths, R., and Korkan, K., "Study of Theoretical and Wind Tunnel Results on Flight Performance Degradation Due to Leading Edge Rime Ice Accretion," *Proceedings of the AIAA 30th Aerospace Sciences Meeting*, AIAA, Washington, DC, 1992 (AIAA Paper 92-0038).

[6]MacArthur, C., "Numerical Simulation of Airfoil Ice Accretion," *Proceedings of the AIAA 21st Aerospace Sciences Meeting*, AIAA, New York, 1983 (AIAA Paper 83-0112).

[7]MacArthur, C., Keller, J., and Luers, J., "Mathematical Modeling of Ice Accretion on Airfoils," *Proceedings of the AIAA 20th Aerospace Sciences Meeting*, AIAA, New York, 1982 (AIAA Paper 82-0284).

[8]Ruff, G., et al., "User's Guide for the NASA Lewis Ice Accretion Prediction Code (LEWICE)," Sverdrup Technology, Inc., LeRC Group, 1986.

[9]Yoeman, K., "Selection of the Critical Icing/Flight Case for an Unprotected Airfoil," *Proceedings of the AIAA 27th Aerospace Sciences Meeting*, AIAA, Washington, DC, 1989 (AIAA Paper 89-0757).

[10]Ranaudo, R., Batterson, J., Reehorst, A., Bond, T., and O'Mara, T., "Effects of Horizontal Tail Ice on Longitudinal Aerodynamic Derivatives," *Journal of Aircraft*, Vol. 28, 1991, pp. 193–199.

[11]Weisend, N., Jr., "Design of an Advanced Pneumatic Deicer for the Composite Rotor Blade," *Journal of Aircraft*, Vol. 26, 1989, pp. 947–950.

[12]Scavuzzo, R., Chu, M., and Kellackey, C., "Impact Ice Stresses in Rotating Airfoils," *Journal of Aircraft*, Vol. 28, 1991, pp. 450–455.

[13]Horne, T., "Weeping Wings," *AOPA Pilot*, Jan. 1984, pp. 36–38.

[14]Newman, R., "Flight Testing a Liquid Ice Protection System on a Single-Engine Airplane," *Proceedings of the General Aviation Aircraft Meeting and Exposition*, 1985 (Society of Automotive Engineers Paper 850923).

[15]Albright, A., "A Summary of NASA's Research on the Fluid Ice Protection System," *Proceedings of the AIAA 23rd Aerospace Sciences Meeting*, AIAA, New York, 1985 (AIAA Paper 85-0467).

[16]Kohlman, D., Schweikhard, W., and Evanich, P., "Icing Tunnel Tests of a Glycol-Exuding Porous Leading Edge Ice Protection System," *Journal of Aircraft*, Vol. 19, 1982, pp. 647–654.

[17]Rosenthal, H., Nelepovitz, D., and Rockholt, H., "Deicing of Aircraft Turbine Engine Inlets," Final Rept., Rohr Industries, Inc., DOT/FAA/CT-87/37, 1988.

[18]Anon., "Anti-Icing Equipment for Aircraft, Heated Surface Type. General Specifications for," MIL-A-9482, Sept. 2, 1954, amended April, 2, 1981.

[19]Yaslik, A., DeWitt, K., and Keith, T., Jr., "Further Developments in Three-Dimensional Numerical Simulation of Electrothermal Deicing Systems," *Proceedings of the AIAA 30th Aerospace Sciences Meeting*, AIAA, Washington, DC, 1992 (AIAA Paper 92-0528).

[20]Fanelli, M., Wright, W., Masiulaniec, K., DeWitt, K., Keith, T., Jr., Cole, R., Wilson, T., Bowen, K., and Martin, C., "Experimental and Numerical Investigation of Anti-Icing Phenomena on a NACA 0012 Assembly," *Proceedings of the AIAA 30th Aerospace Sciences Meeting*, AIAA, Washington, DC, 1992 (AIAA Paper 92-0531).

[21]Bond, T., Shin, J., and Mesander, G., "Advanced Ice Protection Systems Test in the NASA Lewis Icing Research Tunnel," *Proceedings of the 47th Annual Forum and Technology Display*, 1991 (NASA TM 103757).

[22]Martin, C., and Putt, J., "Advanced Pneumatic Impulse Ice Protection System (PIIP) for Aircraft," *Journal of Aircraft*, Vol. 29, 1992, pp. 714–716.

[23]Zumwalt, G., Schrag, R., Bernhart, W., and Friedberg, R., "Electro-Impulse De-Icing Testing Analysis and Design," NASA CR-4175, 1988.

[24]Gien, P., "Flexural Waves Induced by Electro-Impulse Deicing Forces," *Proceedings of the 13th ASME Annual Energy-Sources Technology Conference* (New Orleans, LA), American Society of Mechanical Engineers, New York, 1990, pp. 267–271.

[25]Ross, R., "Electro-Impulse Deicing of the NASA Lewis Altitude Wind Tunnel Turning Vanes," *Journal of Aircraft*, Vol. 25, 1988, pp. 499–501.

[26]Schrag, R., and Zumwalt, G., "Electro-Impulse Deicing: Concept and Electrodynamic Studies," *Proceedings of the AIAA 22nd Aerospace Sciences Meeting*, AIAA, New York, 1984 (AIAA Paper 84-0021).

[27]Bernhart, W., and Zumwalt, G., "Electro-Impulse Deicing: Structural Dynamic Studies, Icing Tunnel Tests and Applications," *Proceedings of the AIAA 22nd Aerospace Sciences Meeting*, AIAA, New York, 1984 (AIAA Paper 84-0022).

[28]Zumwalt, G., Friedberg, R., and Schwartz, J., "Electro-Impulse De-Icing Research: Fatigue and Electromagnetic Interference Tests," Federal Aviation Administration Rept. DOT/FAA/CT-88/27, 1989.

[29]Zieve, P., Huffer, B., and Ng, J., "Electromagnetic Emissions from a Modular Low Voltage Electro-Impulse De-Icing System," Federal Aviation Administration Rept. DOT/FAA/CT-88/31; also *Proceedings of the AIAA 27th Aerospace Sciences Meeting*, AIAA, Washington, DC, 1989 (AIAA Paper 89-0758).

[30]Zumwalt, G., "Electromagnetic Emissions from an Electro-Impulse Deicing System in a Composite Wing Equipped with Lightning Protection," Federal Aviation Administration Rept. DOT/FAA/CT-TN90/32, 1991.

[31]Zieve, P., Ng, J., and Friedberg, R., "Suppression of Radiating Harmonics in Electro-Impulse Deicing Systems," Federal Aviation Administration Rept. DOT/FAA/CT-TN90/33, 1991.

[32]Smith, S., and Zieve, P., "Thin Film Eddy Current Impulse Deicer," *Proceedings of the AIAA 28th Aerospace Sciences Meeting*, AIAA, Washington, DC, 1990 (AIAA Paper 90-0761).

[33]Nordwall, B., "NASA Tests Electro-Expulsive Deicer that Could Protect F/A-18 Engines," *Aviation Week & Space Technology*, Aug. 3, 1987, pp. 89–93.

[34]Theodorsen, T., "Theory of Wing Sections of Arbitrary Shape," NACA Rept. 411, 1932.

[35]Theodorsen, T., and Garrick, I., "General Potential Theory of Arbitrary Wing Sections," NACA Rept. 452, 1933.

[36]Bragg, M., "Rime Ice Accretion and Its Effect on Airfoil Performance," NASA CR-165599, 1982.

[37]Bragg, M., and Gregorek, G., "Aerodynamic Characteristics of Airfoils with Ice Accretions," *Proceedings of the AIAA 20th Aerospace Sciences Meeting*, AIAA, New York, 1982 (AIAA Paper 82-0282).

[38]Bragg, M., and Gregorek, G., "An Analytical Evaluation of the Icing Properties of Several Low and Medium Speed Airfoils," *Proceedings of the AIAA 21st Aerospace Sciences Meeting*, AIAA, New York, 1983 (AIAA Paper 83-0109).

[39]Bragg, M., "Effect of Geometry on Airfoil Icing Characteristics," *Journal of Aircraft*, Vol. 21, 1984, pp. 505–511.

[40]Bragg, M., "Predicting Rime Ice Accretion on Airfoils," *AIAA Journal*, Vol. 23, 1985, pp. 381–387.

[41]Miller, T., Korkan, K., and Shaw, R., "Analytical Determination of Propeller Performance Degradation Due to Ice Accretion," *Journal of Aircraft*, Vol. 25, 1987, pp. 768–775.

[42]Smith, A., "The Panel Method: Its Original Development," *Applied Computational Aerodynamics*, AIAA, Washington, DC, 1990, pp. 3–17.

[43]Ruff, G., and Berkowitz, B., "User's Manual for the NASA Lewis Ice Accretion Prediction Code (LEWICE)," NASA CR 185129, 1990.

[44]Cebeci, T., "Calculation of Flow over Iced Airfoils," *AIAA Journal*, Vol. 27, 1989, pp. 853–861.

[45]Hess, J., and Valarezo, W., "Application of an Advanced Panel Method to Aerodynamic Problems of Aircraft Design," *Panel Methods in Fluid Mechanics with Emphasis on Aerodynamics, Proceedings of the 3rd GAMM-Seminar*, Kiel, Germany, 1987, pp. 79–90.

[46]Hess, J., and Smith, A., "Calculation of Potential Flow About Arbitrary Bodies," *Progress in Aeronautical Sciences*, Vol. 8, Pergamon, Oxford, England, UK, 1966, pp. 1–138.

[47]Frost, W., Chang, H., and Kimble, K., "Particle Trajectory Computer Program for Icing Analysis of Axisymmetric Bodies," NASA-CR-189134, 1982.

[48]Hedde, T., and Guffond, D., "Development of a Three-Dimensional Icing Code, Comparison with Experimental Shapes," *Proceedings of the AIAA 30th Aerospace Sciences Meeting*, AIAA, Washington, DC, 1992 (AIAA Paper 92-0041).

[49]Shapiro, A., *The Dynamics and Thermodynamics of Compressible Fluid Flow*, Vol. 1, Wiley, New York, 1953.

[50]Potapczuk, M., "LEWICE/E: A Euler Based Ice Accretion Code," *Proceedings of the AIAA 30th Aerospace Sciences Meeting*, AIAA, Washington, DC, 1992 (AIAA Paper 92-0037).

[51]Cebeci, T., Chen, H., and Alemdaroglu, N., "Fortified LEWICE with Viscous Effects," *Journal of Aircraft*, Vol. 28, 1991, pp. 564–571.

[52]Shin, J., Berkowitz, B., Chen, H., and Cebeci, T., "Prediction of Ice Shapes and Their Effect on Airfoil Drag," *Journal of Aircraft*, Vol. 31, No. 2, 1994, pp. 263–270.

[53]Paraschivoiu, I., Tran, P., and Brahimi, M., "Prediction of Ice Accretion with Viscous Effects on Aircraft Wings," *Journal of Aircraft*, Vol. 31, 1994, pp. 855–861.

[54]Anderson, D., Tannehill, J., and Pletcher, R., *Computational Fluid Mechanics and Heat Transfer*, Hemisphere, New York, 1984.

[55]Scott, J., Hankey, W., Giessler, F., and Gielda, T., "Navier-Stokes Solution to the Flowfield over Ice Accretion Shapes," *Journal of Aircraft*, Vol. 25, 1988, pp. 710–716.

[56]Kohlman, D., and Albright, A., "A Method of Predicting Flow-Rates Required to Achieve Anti-Icing Performance with a Porous Leading Edge Ice Protection System," NASA-CR-168213, 1983.

[57]Hansman, R., Jr., and Turnock, S., "Investigation of Surface Water Behavior During Glaze Ice Accretion," *Journal of Aircraft*, Vol. 26, 1989, pp. 140–147.

[58]Messinger, B. L., "Equilibrium Temperature of an Unheated Icing Surface as a Function of Airspeed," *Journal of the Aeronautical Sciences*, Vol. 20, 1953, pp. 29–41.

[59]Al-Khalil, K., Keith, T., and De Witt, K., "Development of an Improved Model for Runback Water on Aircraft Surfaces," *Proceedings of the AIAA 30th Aerospace Sciences Meeting*, AIAA, Washington, DC, 1992 (AIAA Paper 92-0042).

[60]Pais, M., Singh, S., and Zou, L., "Determination of the Local Heat Transfer Characteristics on Simulated Smooth Glaze Ice Accretions on a NACA 0012 Airfoil," *Proceedings of the AIAA 26th Aerospace Sciences Meeting*, AIAA, Washington, DC, 1988 (AIAA Paper 88-0292).

[61]Yamaguchi, K., and Hansman, R., Jr., "Heat Transfer on Accreting Ice Surfaces," *Journal of Aircraft*, Vol. 29, 1992, pp. 108–113.

[62]Bragg, M., Gregorek, G., and Lee, J., "Airfoil Aerodynamics in Icing Conditions," *Journal of Aircraft*, Vol. 23, 1986, pp. 76–81.

[63]Khodadoust, A., and Bragg, M., "Aerodynamics of a Finite Wing with Simulated Ice," *Journal of Aircraft*, Vol. 32, No. 1, 1995, pp. 137–144.

[64]Gray, V., "Prediction of Aerodynamic Penalties Caused by Ice Formations on Various Airfoils," NASA-TN-D-2166, 1964.

[65]Flemming, R., and Lednicer, D., "High Speed Ice Accretion on Rotorcraft Airfoils," NASA-CR-3910, 1985.

[66]Smetana, F., Summey, D., Smith, N., and Carden, R., "Light Aircraft Lift, Drag, and Moment Prediction—A Review and Analysis," NASA-CR-2523, 1975.

[67]Eppler, R., and Somers, D., "A Computer Program for the Design and Analysis of Low-Speed Airfoils," NASA-TM-80210, 1980.

[68]Bristow, D., "Multi-Element Airfoil Inviscid Analysis and Design Program (Version 1): User Instructions," McDonnell Aircraft Co., St. Louis, MO, 1980.

[69]Keith, T., Jr., DeWitt, K., Wright, W., and Masiulaniec, K., "Overview of Numerical Codes Developed for Predicted Electrothermal De-Icing of Aircraft Blades," *Proceedings of the AIAA 26th Aerospace Sciences Meeting*, AIAA, Washington, DC, 1988 (AIAA Paper 88-0288).

[70]Wright, W., Keith, T., Jr., and DeWitt, K., "Transient Two-Dimensional Heat Transfer Through a Composite Body with Application to De-Icing of Aircraft Components," AIAA, Washington, DC, 1988 (AIAA Paper 88-2260).

[71]Henry, R., "Development of an Electrothermal De-Icing/Anti-Icing Model," *Proceedings of the AIAA 30th Aerospace Sciences Meeting*, AIAA, Washington, DC, 1992 (AIAA Paper 92-0526).

[72]Huang, J., Keith, T., Jr., and DeWitt, K., "Numerical Simulation of an Electrothermal De-Iced Aircraft Surface Using the Finite Element Method," *Proceedings of the AIAA 29th Aerospace Sciences Meeting*, AIAA, Washington, DC, 1991 (AIAA Paper 91-0268).

[73]Wright, W., Keith, T., Jr., and DeWitt, K., "Numerical Analysis of a Thermal Deicer," *Proceedings of the AIAA 30th Aerospace Sciences Meeting*, AIAA, Washington, DC, 1992 (AIAA Paper 92-0527).

[74]Huang, J., Keith, T., Jr., and DeWitt, K., "An Efficient Finite Element Method for Aircraft De-Icing Problems," *Proceedings of the AIAA 30th Aerospace Sciences Meeting*, AIAA, Washington, DC, 1992 (AIAA Paper 92-0532).

[75]Huang, J., Keith, T., Jr., and DeWitt, K., "Investigation of an Electrothermal De-Icer Pad Using a Three-Dimensional Finite Element Simulation," *Proceedings of the AIAA 30th Aerospace Sciences Meeting*, AIAA, Washington, DC, 1993 (AIAA Paper 93-0532).

[76]Huang, J., Keith, T., Jr., and DeWitt, K., "Effect of Curvature in the Numerical Simulation of an Electrothermal De-Icer Pad," *Journal of Aircraft*, Vol. 32, No. 1, 1995, pp. 84–92.

[77]Al-Khalil, K., Keith, T., Jr., DeWitt, K., Nathman, J., and Dietrich, D., "Thermal Analysis of Engine Inlet Anti-Icing Systems," *Proceedings of the AIAA 27th Aerospace Sciences Meeting*, AIAA, Washington, DC, 1989 (AIAA Paper 89-0579).

[78]Schneider, G., and Raw, M., "An Implicit Solution Procedure for Finite Difference Modeling of the Stefan Problem," *AIAA Journal*, Vol. 22, 1984, pp. 1685–1690.

[79]Roelke, R., Keith, T., Jr., and DeWitt, K., "Efficient Numerical Solution of a One-Dimensional Electrothermal Deicer Pad," *Journal of Aircraft*, Vol. 25, 1992, pp. 1087–1105.

[80]Lewis, G., "The Electrodynamic Operation of Electro-Impulse De-Icing Systems," *Proceedings of the AIAA 24th Aerospace Sciences Meeting*, AIAA, New York, 1986 (AIAA Paper 86-0547).

[81]Bernhart, W., and Schrag, R., "Electroimpulse Deicing: Electrodynamic Solution by Discrete Elements," *Journal of Aircraft*, Vol. 26, 1989, pp. 547–553.

[82]Zieve, P., "Low Voltage Electro-Impulse De-Icer," *Proceedings of the AIAA 26th Aerospace Sciences Meeting*, AIAA, Washington, DC, 1988 (AIAA Paper 88-0021).

[83]Scavuzzo, R., Chu, M., Woods, E., Raju, R., and Khatkhate, A., "Finite Element Studies of the Electro Impulse De-Icing System," *Journal of Aircraft*, Vol. 27, 1990, pp. 757–763.

[84]Scavuzzo, R., Chu, M., and Ananthaswamy, V., "Influence of Aerodynamic Forces in Ice Shedding," *Journal of Aircraft*, Vol. 31, 1994, pp. 526–530.

[85]Faghri, A., *Heat Pipe Science and Technology*, Taylor and Francis, Washington, DC, 1995.

[86]Yerkes, K., and Hager, B., "Transient Response of Heat Pipes for Actuator Thermal Management," *Proceedings of the Aerospace Atlantic Conference* (Dayton, OH), 1992 (Society of Automotive Engineers Paper 921024).